# CONTROL OF INVERTER-ASSISTED SINGLE-PHASE INDUCTION GENERATORS

by

Maxwell Myers

A thesis submitted to the faculty of
The University of Utah
in partial fulfillment of the requirements for the degree of

Master of Science

Department of Electrical and Computer Engineering

The University of Utah

December 2012

**The University of Utah Graduate School**

# STATEMENT OF THESIS APPROVAL

The thesis of **Maxwell Myers**

has been approved by the following supervisory committee members:

| | | |
|---|---|---|
| **Marc Bodson** | , Chair | **4/20/12** Date Approved |
| **Faisal Khan** | , Member | **4/05/12** Date Approved |
| **Jake Abbott** | , Member | **4/17/12** Date Approved |

and by **Gianluca Lazzi** , Chair of

the Department of **Electrical and Computer Engineering**

and by Charles A. Wight, Dean of The Graduate School.

# ABSTRACT

This thesis investigates the problem of producing power using a single-phase induction machine. Single-phase induction motors are typically nonsymmetric two-phase motors, also called split-phase motors, with a main winding and an auxiliary winding. We consider the control of power delivered by the main winding through the auxiliary winding. A state-space model of an asymmetric split-phase generator has been developed. This model is used to characterize and identify a 1/3 hp induction machine. The parameters are used to predict suitable operating regions for the generator. It is found that there exists a viable operating region in a band just above the synchronous speed of the motor. Four control algorithms are presented. The first is a simple open-loop algorithm for a sinusoidal reference signal. The second is a controller based on the inverse-G adaptive algorithm. The third is an algorithm featuring an adaptive estimate of the system frequency response. Finally, a PI control method is considered for situations where the phase of the generated voltage does not need to be controlled. Simulated and experimental results are presented for each of the control algorithms. The closed-loop algorithms were able to track a desired reference. These algorithms were also able to reject a disturbance caused by a 20 percent increase in speed.

# TABLE OF CONTENTS

# ACKNOWLEDGMENTS

I would like to thank Dr. Bodson for his invaluable support and patience throughout the course of this project. I would also like to thank Dr. Khan and Dr. Abbott for their input to this project.

This thesis is dedicated to my family who taught me the value of education.

# CHAPTER 1

# INTRODUCTION

## 1.1 Problem Statement

This research focuses on the development of a method to obtain usable electric power from commercially available single-phase induction machines (SPIM). There exists an extensive collection of research papers investigating the phenomenon of self-excitation in induction machines. However, it is difficult to extract power from the machines due to the inherent instability and nonlinearity of the self-excitation phenomenon. The current project considers controlled generation when a signal excitation voltage is applied to the auxiliary phase of a nonsymmetric machine and power is produced on the main winding. The goal of this research is to develop a control algorithm that produces 120 V at 60 Hz across the generating phase of the machine. It is assumed that the speed of the rotor is a measured quantity and can be adjusted close to the synchronous speed.

## 1.2 Importance of the Problem

Single-phase induction machines (SPIM) are one of the most ubiquitous types of power converter. Although they are called single phase machines, most are actually nonsymmetric two-phase machines. They are attractive because they are inexpensive, low-maintenance, and lightweight when compared to their synchronous cousins. An important development of the research is a method to model and identify asymmetric single-phase machines. There are standardized tests for the parametrization of symmetric SPIMs, but no such tests exist for asymmetric machines. The proposed parameter identification method can be applied to any

induction machine and can be automated.

This research in the control of residential power generation using off-the-shelf induction machines is particularly relevant given recent interest in alternative energy technology. Although residential generation solutions exist, single-phase induction generators may provide similar performance at a fraction of the cost. Furthermore, these machines are readily available as surplus or salvage and could be utilized as generators in developing countries where access to electrical power is limited.

## 1.3 Review of Previous Work

The idea of using a voltage-source inverter to control the electrical output of an induction generator was first proposed in a paper by Novotny, Gritter, and Studtmann in 1977 [1]. This paper develops equivalent circuit models for the inverter-generator system. This paper uses an inverter to control the power drawn from a three-phase induction generator operating in the self-excited mode. The paper does not provide any experimental results. Results were obtained much later by Murthy in 1993 [2]. Murthy also extended the analysis to consider self-excited single-phase machines. The work was continued by Olorunfemi Ojo at Tennessee Technological University in a series of papers from 1995 to 2001. Ojo's most significant contribution to the work is to use the inverter to excite the auxiliary phase of the machine [4]. This inverter-assisted topology is qualitatively different than self-excited generation. In this configuration, there is a linear relationship between the voltage applied at the excited phase and the voltage produced by the generating phase. An additional feature of this topology is that control is performed on only a single phase so only one inverter is needed. Furthermore, the voltage generated by the machine will have fewer induced harmonics. In [5], Ojo explores the effect of different loading on this generator's performance. He explores the effect of more advanced modulation schemes in [6]-[8]. Finally, Ojo uses the inverter-generator topology to identify the parameters of an induction

machine [9]. Despite his thorough investigation of this topology, Ojo never attempted closed-loop control of the inverter-generator system.

# CHAPTER 2

# PARAMETER IDENTIFICATION

The first step in any control problem is to develop an accurate representation of the plant. This chapter presents a state-space model of an asymmetric induction machine. This model is then simplified to examine operation when one phase is left open while an excitation voltage is applied across the opposite phase. Two frequency response functions are identified as a function of these state-space parameters. One frequency response corresponds to a winding impedance and the other corresponds to the transmittance from one winding to another. Parameters are determined by fitting measured frequency response functions using least-squares algorithms. Finally, the model is expanded to include parameter identification when an RC load is attached in parallel to the generating winding.

## 2.1 Asymmetric Induction Machine Model

Begin by considering the two-phase induction motor shown in Fig. 1. The rotor windings are assumed to be identical, but the stator windings may be different from each other. The rotor windings typically represent a squirrel-cage rotor, rather than actual windings.

Based on the geometry of the motor, the total flux linkages in the four windings are assumed to be of the form

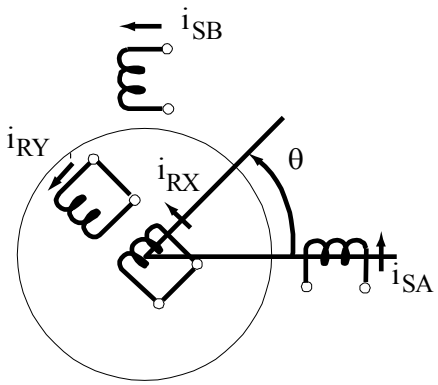


Figure 1: Two-phase induction motor

$$\begin{aligned}
\psi_{SA} &= L_A i_{SA} + M_A \cos(n_p\theta) i_{RX} - M_A \sin(n_p\theta) i_{RY} \\
\psi_{SB} &= L_B i_{SB} + M_B \sin(n_p\theta) i_{RX} + M_A \cos(n_p\theta) i_{RY} \\
\psi_{RX} &= L_R i_{RX} + M_A \cos(n_p\theta) i_{SA} + M_B \sin(n_p\theta) i_{SB} \\
\psi_{RY} &= L_R i_{RY} - M_B \sin(n_p\theta) i_{SA} + M_B \cos(n_p\theta) i_{SB}
\end{aligned} \tag{1}$$

It is assumed that there is no mutual inductance between stator windings A and B or between rotor windings X and Y. The electrical equations for the stator and rotor windings are given by

$$\begin{aligned}
\frac{d\psi_{SA}}{dt} &= v_{SA} - R_A i_{SA} \quad , \frac{d\psi_{SB}}{dt} = v_{SB} - R_B i_{SB} \\
\frac{d\psi_{RX}}{dt} &= v_{RX} - R_R i_{RX} = -R_R i_{RX} \, , \frac{d\psi_{RY}}{dt} = v_{RY} - R_R i_{RY} = -R_R i_{RY}
\end{aligned} \tag{2}$$

where the right side of the last two equations assume that the rotor windings are short-circuited. Combining (1) and (2) gives a set of four equations which may be organized in the following form

$$\begin{pmatrix} L_A & 0 & M_A\cos(n_p\theta) & -M_A\sin(n_p\theta) \\ 0 & L_B & M_B\sin(n_p\theta) & M_B\cos(n_p\theta) \\ M_A\cos(n_p\theta) & M_B\sin(n_p\theta) & L_R & 0 \\ -M_A\sin(n_p\theta) & M_B\cos(n_p\theta) & 0 & L_R \end{pmatrix} \frac{d}{dt}\begin{pmatrix} i_{SA} \\ i_{SB} \\ i_{RX} \\ i_{RY} \end{pmatrix} = \begin{pmatrix} v_{SA} - R_A i_{SA} + n_p\omega M_A(i_{RX}\sin(n_p\theta) + i_{RY}\cos(n_p\theta)) \\ v_{SB} - R_B i_{SB} - n_p\omega M_B(i_{RX}\cos(n_p\theta) - i_{RY}\sin(n_p\theta)) \\ -R_R i_{RX} + n_p\omega(M_A i_{SA}\sin(n_p\theta) - M_B i_{SB}\cos(n_p\theta)) \\ -R_R i_{RY} + n_p\omega(M_A i_{SA}\cos(n_p\theta) + M_B i_{SB}\sin(n_p\theta)) \end{pmatrix} \quad (3)$$

The rotor currents can be described in a coordinate frame attached to the stator, so that

$$\begin{pmatrix} i_{RA} \\ i_{RB} \end{pmatrix} = \begin{pmatrix} \cos(n_p\theta) & -\sin(n_p\theta) \\ \sin(n_p\theta) & \cos(n_p\theta) \end{pmatrix}\begin{pmatrix} i_{RX} \\ i_{RY} \end{pmatrix} \quad (4)$$

Applying this transformation, the electrical equations of the motor become

$$\begin{pmatrix} L_A & 0 & M_A & 0 \\ 0 & L_B & 0 & M_B \\ M_A & 0 & L_R & 0 \\ 0 & M_B & 0 & L_R \end{pmatrix} \frac{d}{dt}\begin{pmatrix} i_{SA} \\ i_{SB} \\ i_{RA} \\ i_{RB} \end{pmatrix} = \begin{pmatrix} v_{SA} - R_A i_{SA} \\ v_{SB} - R_B i_{SB} \\ -R_R i_{RA} - n_p\omega(L_R i_{RB} + M_B i_{SB}) \\ -R_R i_{RB} + n_p\omega(L_R i_{RA} + M_A i_{SA}) \end{pmatrix} \quad (5)$$

## 2.2 Parameter Identification without Load

Now, consider operation on a single phase, A, with the other phase left open. Thus, $i_{SB} = 0$. The speed is assumed to be constant. The system can then be studied with Laplace transforms, so that

$$\begin{pmatrix} s_{LA} + R_A & sM_A & 0 \\ sM_A & sL_R + R_R & n_p\omega L_R \\ -n_p\omega M_A & -n\,p\omega L_R & sL_R + R_R \end{pmatrix}\begin{pmatrix} i_{SA} \\ i_{RA} \\ i_{RB} \end{pmatrix} = \begin{pmatrix} v_{SA} \\ 0 \\ 0 \end{pmatrix} \quad (6)$$

while

$$v_{SB} = sM_B i_{RB} \quad (7)$$

Let the determinant of the matrix be

$$D(s) = (sL_A + R_A)((sL_R + R_R)^2 + (n_p\omega L_R)^2) - sM_A^2(s(sL_R + R_R) + (n_p\omega)^2 L_R) \quad (8)$$

Then

$$\begin{pmatrix} i_{SA} \\ i_{RA} \\ i_{RB} \end{pmatrix} = \begin{pmatrix} (sL_R+R_R)^2+(n_p\omega L_R)^2 \\ -M_A(s(sL_R+R_R)+(n_p\omega)^2 L_R) \\ n_p\omega M_A R_R \end{pmatrix} \frac{v_{SA}}{D(s)} \tag{9}$$

and

$$v_{SA}=\frac{D(s)}{(sL_R+R_R)^2+(n_p\omega L_R)^2} i_{SA}, i_{RB}=\frac{n_p\omega M_A R_R}{(sL_R+R_R)^2+(n_p\omega L_R)^2} i_{SA} \tag{10}$$

If we define the impedance $Z_A(s)$ of phase A and the transmittance $G_{AB}(s)$ from the current in A to the voltage in B, we have

$$v_{SA}=Z_A(s) i_{SA}, v_{SB}=G_{AB}(s) i_{SA} \tag{11}$$

where

$$Z_A(s)=(sL_A+R_A)-sM_A^2\frac{s(sL_R+R_R)+(n_p\omega)^2 L_R}{(sL_R+R_R)^2+(n_p\omega L_R)^2} \tag{12}$$

$$G_{AB}(s)=\frac{sn_p\omega M_A M_B R_R}{(sL_R+R_R)^2+(n_p\omega L_R)^2} \tag{13}$$

Knowing the two transfer functions $Z_A$ and $G_{AB}$, it is possible to determine the following five constants

$$C_1=\frac{n_p\omega M_A M_B R_R}{L_R^2}, C_2=\frac{R_R}{L_R}, C_3=(n_p\omega)^2, C_4=L_A, C_5=R_A \tag{14}$$

Indeed, then transfer functions (18) and (19) can be expressed as

$$Z_A(s)=(C_4 s+C_5)-\frac{C_1 s}{C_2\sqrt{C_3}}\frac{s^2+C_2 s+C_3}{(s+C_2)^2+C_3} \tag{15}$$

$$G_{AB}(s)=\frac{C_1 s}{(s+C_2)^2+C_3} \tag{16}$$

and the constants $C_1$ … $C_5$ are uniquely determined from the transfer functions. For nonsymmetric motors, phases A and B can be swapped to obtain two more parameters: $R_B$ and $L_B$ (as well as validation of the two common parameters, $C_1$ and $C_2$).

First, the method was tested with a symmetric machine so that its results could be

compared to those of conventional methods. The symmetrical split-phase induction motor was mechanically coupled to a dc motor. The test motor had the nameplate data given in Table 1.

A sinusoidal excitation voltage was applied to phase A of the generator and, for a fixed mechanical speed, this excitation frequency was swept from 5 Hz to 100 Hz. For each excitation frequency, the current through phase A and the voltage generated across phase B were measured. The magnitude and the phase of these signals at the excitation frequency were calculated on a data acquisition and processing board.

Two tests were performed in order to demonstrate the repeatability of the technique for different speeds. The first test was performed at 1200 RPM and the second at 3600 RPM. For each test, Bode plots of the measured impedance and transmittance were prepared. Transfer functions (15) and (16) were manually fitted to the data. The resulting Bode plots are displayed in Figs. 2 and 3.

From the definitions in (14), four motor parameters can be identified. Note that all of the parameters of a squirrel-cage induction machine cannot be independently determined. The parameters are displayed in Tables 2 and 3. For comparison, the parameters of the motor obtained using classical standstill and synchronous tests are shown in Table 4. Agreement between the results is very good.

A set of tests was also performed for an asymmetric machine at 2400 RPM. The resulting Bode plot with the excitation applied across the auxiliary winding is shown in Figure 4. The Bode plot with the excitation across the main winding is shown in Figure 5. Each fit was obtained using a least-squares algorithm. The parameters are displayed in Tables 5 and 6.

TABLE 1. NAMEPLATE OF SYMMETRICAL MOTOR

| Volts | Phases | Power | Speed |
|---|---|---|---|
| 24 VAC | 1 | 7.5 W | 3350 RPM |

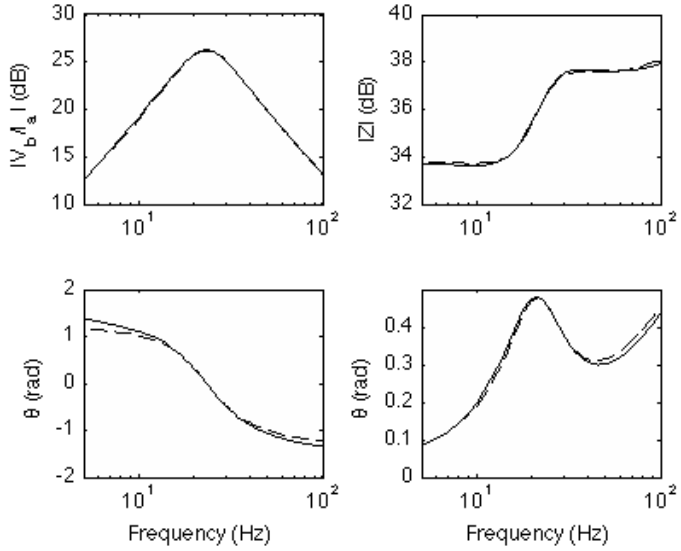


Figure 2: Fit of magnitude and phase of transmittance (left) and impedance (right) data for 1200 RPM. The data are shown by the dotted line, the fit is shown by the solid line.

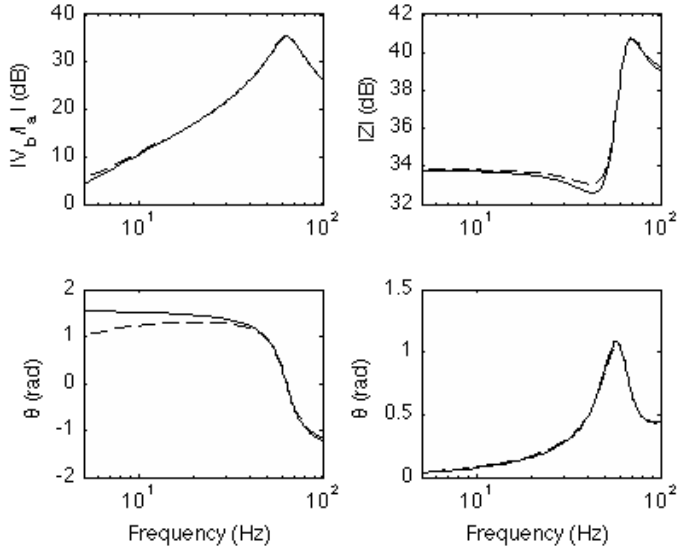


Figure 3: Fit of magnitude and phase of impedance (top) and transmittance (bottom) data for 3600 RPM. The data are shown by the dotted line, the fit is shown by the solid line.

TABLE 2. MEASURED PARAMETERS FOR 1200 RPM

| $R_A$ | $L_A$ | $R_R/L_R$ | $M^2/L_R$ |
|---|---|---|---|
| 48.9 Ω | 0.365 H | 69.0 Ω/H | 0.316 H |

TABLE 3. MEASURED PARAMETERS FOR 3600 RPM

| $R_A$ | $L_A$ | $R_R/L_R$ | $M^2/L_R$ |
|---|---|---|---|
| 48.9 Ω | 0.350 H | 69.0 Ω/H | 0.302 H |

TABLE 4. PARAMETERS MEASURED USING CLASSICAL TESTS

| $R_A$ | $L_A$ | $R_R/L_R$ | $M^2/L_R$ |
|---|---|---|---|
| 49.5 Ω | 0.332 H | 72.3 Ω/H | 0.280 H |

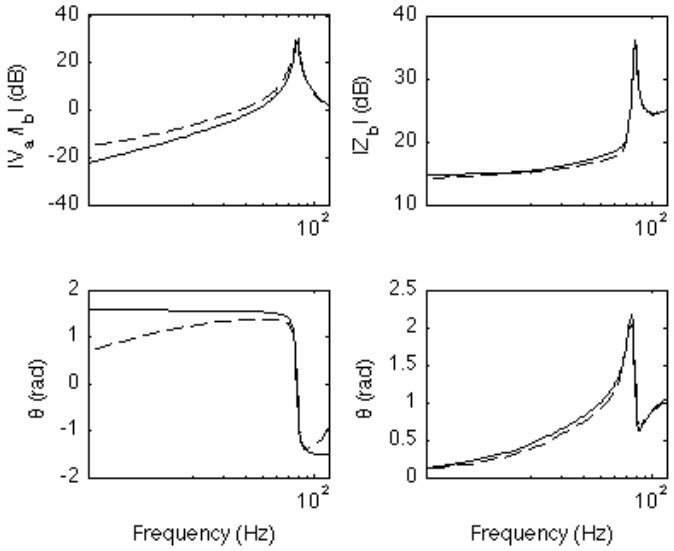


Figure 4: Fit of magnitude and phase of impedance (right) and transmittance (left) data for auxiliary-winding excitation. The rotor velocity was 2400 RPM.

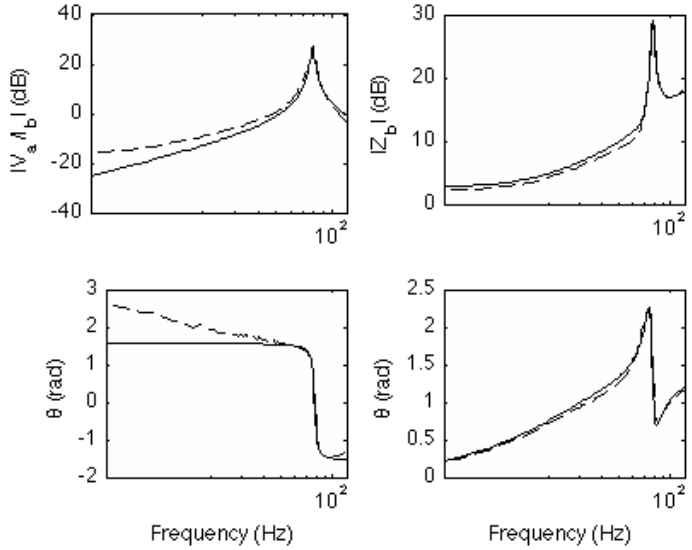


Figure 5: Fit of magnitude and phase of impedance (right) and transmittance (left) data for main-winding excitation. The rotor velocity was 2400 RPM.

TABLE 5. PARAMETERS OBTAINED USING AUXILIARY-WINDING EXCITATION

| $R_A$ | $L_A$ | $R_R/L_R$ | $M_A^2/L_R$ | $M_AM_B/L_R$ |
|---|---|---|---|---|
| 5.38 Ω | 0.199 H | 0.103 Ω / H | 0.177 H | 0.098 H |

TABLE 6. PARAMETERS OBTAINED USING MAIN-WINDING EXCITATION

| $R_B$ | $L_B$ | $R_R/L_R$ | $M_B^2/L_R$ | $M_AM_B/L_R$ |
|---|---|---|---|---|
| 1.34 Ω | 0.122 H | 0.136 Ω / H | 0.113 H | 0.096 H |

## 2.3 Generator Model with Load

Next, consider operation when a load is connected in parallel with the generator. Adding a capacitor *C* and a resistor *R* in parallel to phase B of the system described by (5) gives the following modified equations.

$$E\frac{dx}{dt} = Fx + Gu \tag{17}$$

where

$$E=\begin{pmatrix} L_A & 0 & M_A & 0 & 0 \\ 0 & L_B & 0 & M_B & 0 \\ M_A & 0 & L_R & 0 & 0 \\ 0 & M_B & 0 & L_R & 0 \\ 0 & 0 & 0 & 0 & C \end{pmatrix}, x=\begin{pmatrix} i_{SA} \\ i_{SB} \\ i_{RA} \\ i_{RB} \\ v_{SB} \end{pmatrix}$$

$$F=\begin{pmatrix} -R_A & 0 & 0 & 0 & 0 \\ 0 & -R_B & 0 & 0 & 1 \\ 0 & -n_p\omega M_B & -R_R & -n_p\omega L_R & 0 \\ n_p\omega M_A & 0 & n_p\omega L_R & -R_R & 0 \\ 0 & -1 & 0 & 0 & -1/R_L \end{pmatrix} \tag{18}$$

$$G=\begin{pmatrix} 1 \\ 0 \\ 0 \\ 0 \\ 0 \end{pmatrix}, u=v_{SA}$$

In the Laplace domain, the vector transfer function $H(s)$ from $V_{SA}(s)$ to $X(s)$ is given by

$$H(s)=(Es-F)^{-1}G \tag{19}$$

# CHAPTER 3

# OPERATING CONDITIONS

The next step of the research is the identification of viable operating regions. A region is considered viable if more electrical power is produced than consumed. The size of the viable region is determined by several factors, including load, capacitance, and mechanical frequency. The large number of variables involved makes the identification of these regions non-trivial. Once a viable region is identified, an operating point within the region must be selected. Operating points could be chosen to provide maximum power, to provide optimum efficiency, or to satisfy other design requirements.

This chapter uses the model developed in the previous section to estimate the viable region of an induction generator with an RC load. The simulation is confirmed with experimental power data. The final section of the chapter argues for operating the system around the point where the real power consumed by the excited phase is zero.

## 3.1 Viable Region Estimation

The transfer function defined in (19) can be used to estimate the power generated by the machine. Assuming a sinusoidal voltage is applied to winding A,

$$v_{SA}(t) = A\sin(\omega_e t) \tag{20}$$

The following power variables can be computed.

$$P_A = \frac{A^2}{2} R[H_1(j\omega_e)] \tag{21}$$

$$Q_A = \frac{-A^2}{2} I[H_1(j\omega_e)] \tag{22}$$

$$P_B = \frac{A^2}{2} R[H_2(j\omega_e)H_5(-j\omega_e)] \quad (23)$$

$$Q_B = \frac{-A^2}{2} I[H_2(j\omega_e)H_5(-j\omega_e)] \quad (24)$$

These transfer functions are dependent on electrical frequency, mechanical frequency, load resistance and load capacitance. In order to restrict the design space, the electrical frequency was selected to be 60 Hz and $V_{SB}$ = 110 $V_{pk}$. The load resistance was chosen to be $R_L$ = 100 Ω. This was a choice of necessity as the converter used to drive the prime mover began to behave unpredictably at heavier loads. A load capacitor was placed in parallel with the load resistance, C = 200 μF. The size of the capacitor was selected based on an estimate of the reactive power requirements of the generating phase. This leaves the mechanical frequency, $\omega$, as the only undetermined parameter.

Using Matlab, values of $P_A$, $Q_A$, $P_B$, and $Q_B$ were calculated for a range of $\omega$. Parameters for the calculation were taken from Table 5. The total power generated by both phases of the machine is shown in Figure 6. The computation predicts a viable region just above the synchronous speed of the generator, 188.5 rad/sec. The region is approximately 30 rad/sec wide and peak power is delivered at approximately 207 rad/sec. The real and reactive power of the excited phase is shown in Figure 7. It is important to note that the computation predicts that power can be either consumed or generated by the excited phase.

## 3.2 Verification of Power Curves

In order to confirm the computation, an experiment was performed. Phase A of the induction generator was connected to the grid via a variac. The mechanical frequency of the machine was manually adjusted using a laser tachometer and then the generated voltage was regulated to 110 $V_{pk}$. This procedure was performed for ten speeds above the synchronous speed of the motor. At each point, the power consumption of the machine was measured using a

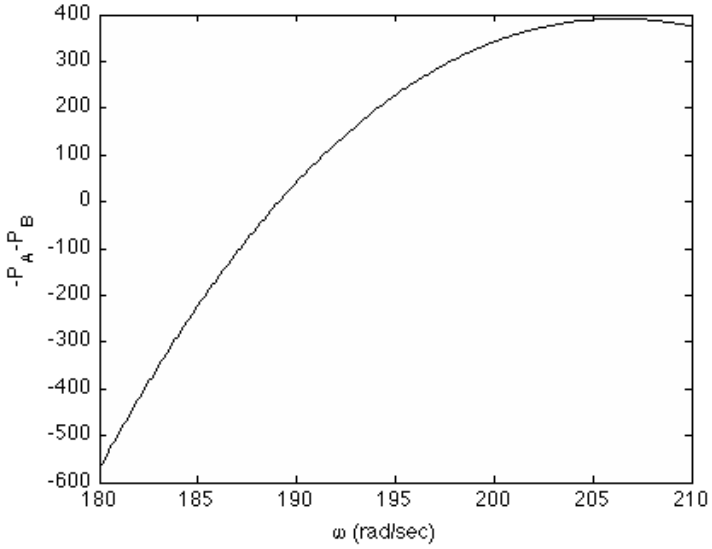


Figure 6: Predicted total power generated by an asymmetrical induction machine

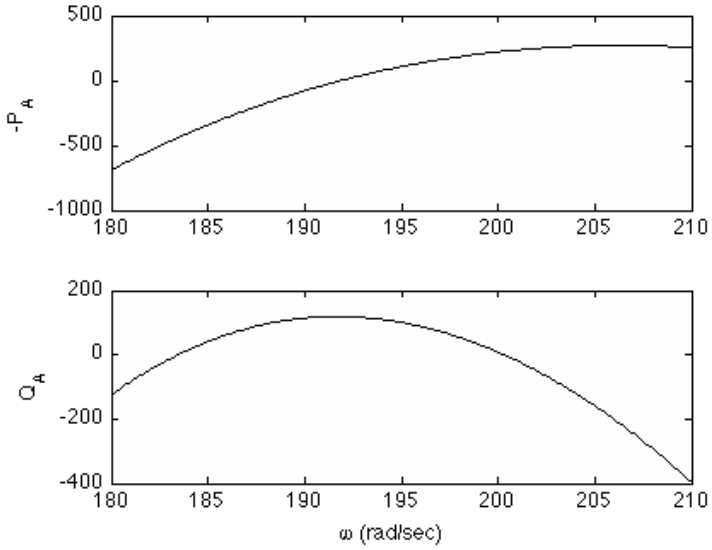


Figure 7: Predicted real and reactive power consumed by phase A

Voltech PM1000 Power Analyzer. The total power generated is plotted alongside the predicted values in Figure 8. Figure 9 shows the active and reactive power consumed by the excited phase.

The data are in good agreement with the predicted values. The data follow the trend of the simulation. The maximum deviation from the predicted total power generated is 32 percent.

## 3.3 Selection of Operation Point

Once the feasible region is identified, the next step is to choose an operating point within the region. As shown in Figure 7, the point $P_A = 0$ appears within the range of viable frequencies at approximately $\omega = 193.25$ rad/sec. This is an attractive operating point since the excited phase does not consume any real power. A battery could supply the reactive power to the phase. Changes to the state of charge of the battery could be obtained through small speed adjustments around the operating point. This is especially significant if the generator is designed to be operated off-grid. This operating point is also attractive because the excited phase does not generate any real power. If a standard off-the-shelf amplifier is used for the controller, it will not be able to regenerate power. Power flowing back to the amplifier will cause significant distortions in the input voltage. The alternative to these amplifiers is to design an ad hoc power converter to control power flow between the battery and generator. This is unattractive since it would increase the cost and complexity of the design. Due to these properties, $P_A = 0$ was chosen as the operating point for the control design.

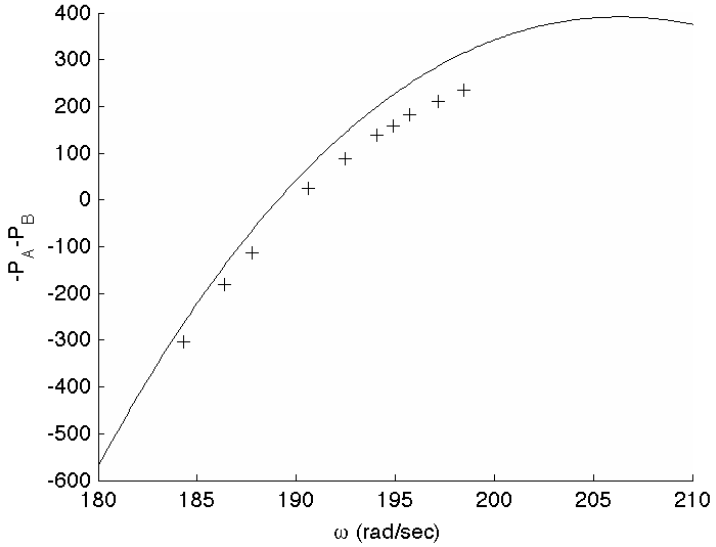


Figure 8: Total power generated by the induction machine

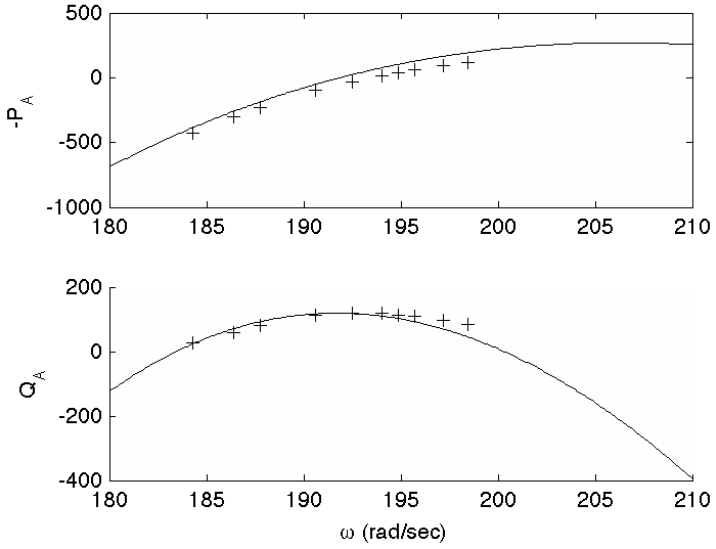


Figure 9: Real and reactive power generated by phase A

# CHAPTER 4

# CONTROL DEVELOPMENT

The final phase of the project was the development of methods to produce a controlled voltage across the generating phase of the machine. This problem presents several challenges. First, the system is highly resonant. This means that a pair of poles is near the jω-axis and the system is close to instability. Another challenge is that transfer function of the plant is dependent on the mechanical velocity. Changes in this velocity can cause the system to depart significantly from original conditions. Finally, the model includes equations for the rotor currents. In practice, these currents cannot be measured. The robust controller must function without knowledge of these currents and uncertainties in the parameters, speed, and load.

Four controllers have been considered: an open-loop controller, two adaptive controllers and a PI controller. The first three controllers are designed to match the amplitude and phase of a reference signal. The ability to track both the amplitude and the phase is important in order to connect the generator to the grid. The PI controller is designed to generate a sinusoidal voltage at a desired amplitude. This method is applicable to systems operating as stand-alone generators where phase is not a consideration. All four methods are discussed in detail below. The analyses are based on steady-state sinusoidal responses.

## 4.1 Open-Loop Control

The system is assumed to be described by

$$y(t) = P(s)[u(t)] \tag{25}$$

where $y(t)$ is the plant output, $u(t)$ is the control input, and $P(s)[(\cdot)]$ denotes the time-domain

output of the plant with transfer function $P(s)$. In this context, $u$ is the voltage applied to the auxiliary phase ($v_{SA}$) and $y$ is the voltage at the main phase ($v_{SB}$). The plant is assumed to be stable. The objective is for the plant output to track a sinusoidal reference signal

$$r(t)=r_c\cos(\omega_e t)+r_s\sin(\omega_e t) \tag{26}$$

where $r_c$, $r_s$ are reference parameters determining the magnitude and phase of the reference signal, and $\omega_e$ is the frequency of the reference signal. Specifically,and $\omega_e=2\pi 60$. The control signal is chosen to be

$$u(t)=u_c\cos(\omega_e t)+u_s\sin(\omega_e t) \tag{27}$$

where $u_c$, $u_s$ are control parameters to be determined.

For fixed control parameters, the steady-state output of the plant is

$$y_{ss}=P_R(u_c\cos(\omega_e t)+u_s\sin(\omega_e t))+P_I(-u_c\sin(\omega_e t)+u_s\cos(\omega_e t)) \tag{28}$$

where $P_R$, $P_I$ are the real and imaginary parts of the plant's frequency response evaluated at $\omega_e$. It follows that $y_{ss}(t) = r(t)$ for all $t$ if $u_c$, $u_s$ are equal to the so-called nominal control parameters

$$\begin{pmatrix} u_c^* \\ u_s^* \end{pmatrix}=G^{*-1}\begin{pmatrix} r_c \\ r_s \end{pmatrix} \tag{29}$$

where $G^*$ is given by

$$G^*=\begin{pmatrix} P_R & P_I \\ -P_I & P_R \end{pmatrix} \tag{30}$$

In practice, equation (27) may be implemented as a control algorithm with

$$\begin{pmatrix} u_c \\ u_s \end{pmatrix}=G^{-1}\begin{pmatrix} r_c \\ r_s \end{pmatrix} \tag{31}$$

where $G$ is an estimate of the matrix $G^*$. This algorithm will work well if precise estimates of $P_R$ and $P_I$ are known. Estimates can be computed from the model of section 3.1, but depend on speed and load parameters.

## 4.2 Adaptive Algorithm for Known Plant

The first adaptive method is the so-called inverse-G adaptive algorithm [16], which is a special case of the filtered-x LMS algorithm in signal processing. This method searches for control parameters that minimize the error between the reference signal and the plant output. For this purpose, it is convenient to define

$$r_v=\begin{pmatrix} r_c \\ r_s \end{pmatrix}, u_v=\begin{pmatrix} u_c \\ u_s \end{pmatrix}, w(t)=\begin{pmatrix} \cos(\omega_e t) \\ \sin(\omega_e t) \end{pmatrix} \tag{32}$$

so that

$$r(t)=w^T(t)r_v, u(t)=w^T(t)u_v, y_{ss}=w^T(t)G^* u_v \tag{33}$$

in steady state. The adaptive algorithm for $u_v$ is then defined as

$$\dot{u}_v(t)=2g\,G^{-1}w(t)(r(t)-y(t)) \tag{34}$$

where $g > 0$ is an arbitrary adaptation gain to be adjusted for optimal performance.

A motivation for (34) can be found using the theory of averaging. A simplified explanation follows. Approximating $y$ by its steady-state value for fixed control parameters

$$r(t)-y(t)\simeq w^T(t)(r_v-G^* u_v) \tag{35}$$

Neglecting sinusoidal terms of frequency $2\omega_e$ (to be "averaged" by the differential equation for $u_v$), one has

$$2\,w(t)w^T(t)\simeq I \tag{36}$$

where $I$ is the identity matrix and therefore

$$2\,w(t)(r(t)-y(t))\simeq r_v-G^* u_v \tag{37}$$

With these approximations

$$\dot{u}_v(t)=g\,G^{-1}G^*(u_v^*-u_v) \tag{38}$$

In ideal conditions ($G = G^*$),

$$\dot{u}_v(t)=g(u_v^*-u_v) \tag{39}$$

so that the control vector converges to the nominal vector with the dynamics of a first-order system with dimension 2 and poles at $s = -g$. The advantage of the algorithm is that convergence to the nominal vector still occurs if $G = G^*$, as long as stability is preserved. In general, the stability of the system is determined by the roots of

$$\det\left(s\,I - g\,G^{-1}\,G^{*}\right) = 0 \tag{40}$$

which remain in the open left-half plane if $G$ is sufficiently close to $G^*$.

## 4.3 Adaptive Algorithm with Plant Adaptation

The second adaptive algorithm is a simplified form of the algorithm by Pigg and Bodson [17]. This simplification occurs because the reference parameters $r_c$, $r_s$ are known and do not need to be estimated. The algorithm is obtained by defining a vector of plant parameter estimates $x$, whose nominal value is

$$x^{*} = \begin{pmatrix} P_R \\ P_I \end{pmatrix} \tag{41}$$

The control law is defined from the parameter estimates as if they were the nominal parameters, i.e.,

$$u_v = G^{-1}\,r_v \tag{42}$$

with

$$G = \begin{pmatrix} x_1 & x_2 \\ -x_2 & x_1 \end{pmatrix} \tag{43}$$

Then, (35) can be rewritten as

$$2\,w(t)\left(r(t) - y(t)\right) \simeq r_v - W\,x^{*} \tag{44}$$

where

$$W = \begin{pmatrix} u_c & u_s \\ -u_s & u_c \end{pmatrix} = \frac{1}{x_1^2 + x_2^2}\begin{pmatrix} x_1 r_c - x_2 r_s & x_1 r_s + x_2 r_c \\ x_1 r_s + x_2 r_c & -x_1 r_c + x_2 r_s \end{pmatrix} \tag{45}$$

Next, define the error signal

$$e_a = W\,x - r_v + 2\,w(t)\,(r(t) - y(t)) \tag{46}$$

Within approximations made earlier, the error signal is equal to

$$e_a = W\,(x - x^*) \tag{47}$$

so that the error vector $e_a$ is related linearly to the parameter error, and standard gradient or least-squares algorithms can be used for parameter estimation. For example, a gradient algorithm is given by

$$\dot{x} = -g\,W^T e_a \tag{48}$$

where $g > 0$ is an adaptation gain to be selected arbitrarily. The algorithm is nonlinear because $W$ is a function of $x$. However, it is guaranteed to be stable because

$$\begin{aligned} \frac{d}{dt}|x - x^*|^2 &= -2\,g\,(x - x^*)^T W^T e_a \\ &= -2\,g\,(W\,(x - x^*)^T W\,(x - x^*)) \\ &= -2\,g\,|W\,(x - x^*)|^2 \\ &\le 0 \end{aligned} \tag{49}$$

Further, the parameter error and the tracking error converge to zero if $W$ is nonsingular, which requires that $r_c$ or $r_s \neq 0$. There is a potential problem in the computation of $u$ if $x_1^2 + x_2^2 = 0$, but it can be avoided by replacing the computation of $u_v$ by

$$u_v = \frac{1}{\max\,(\varepsilon\,,\, x_1^2 + x_2^2)} \begin{pmatrix} x_1 r_c - x_2 r_s \\ x_1 r_s + x_2 r_c \end{pmatrix} \tag{50}$$

where $\varepsilon$ is a small positive number such that $\varepsilon < x_1^{*2} + x_2^{*2}$.

## 4.4 PI Control

The previous three controllers considered tracking the magnitude and phase of a reference sinusoid. The controller design can be simplified when the phase is unimportant. A straightforward approach is to calculate the difference between a measured amplitude and a

reference amplitude and then apply the techniques of PID controller design. The problem is reduced to calculating a continuous, accurate estimate of the amplitude of the generated voltage.

One solution to obtain the envelope of a signal is to use a diode detector. These types of detectors were common in early AM radios. Unfortunately these types of detectors are sensitive to noise and have an asymmetric voltage response. The diode detector was found to be unsuitable for this application due to these drawbacks.

Another way of calculating the amplitude is to define an estimate of the generated voltage,

$$\hat{y}(t) = y_c \cos(\omega t) + y_s \sin(\omega t) \tag{51}$$

The values of $y_c$ and $y_s$ are updated by performing the continuous averaging defined below.

$$\dot{y}_c = g(y(t) - \hat{y}(t))\cos(\omega t) \tag{52}$$

$$\dot{y}_s = g(y(t) - \hat{y}(t))\sin(\omega t) \tag{53}$$

where $g > 0$ is a gain that represents the "memory" of the filter. The amplitude of the estimate is simply $Y = \sqrt{(y_c^2 + y_s^2)}$.

# CHAPTER 5

# SYSTEM SIMULATION

The next step in the design process was to develop simulation models to test the validity of the control algorithms. This chapter presents Simulink simulations of each of the control methods discussed in the previous chapter. The simulations all use a solver based on the Euler method. The step size of the solver was set to 0.0001 seconds in order to correspond to the sampling frequency of the experimental equipment. The reference signal was chosen to be

$$r(t) = r_c \cos(\omega t) + r_s \sin(\omega t) = 110 \cos(2\pi 60 t) \tag{54}$$

Note that the amplitude of the reference voltage is 110 $V_{pk}$ instead of 110 $V_{RMS}$. The smaller reference was used because the amplifier used for the experiments began to saturate at 150 $V_{pk}$. The voltage was slightly derated to avoid clipping leading to unwanted distortion.

The first step was to develop a suitable model of the induction generator. The state-space model of the generator presented in 2.3 was coded in Simulink. This system is shown in Figure 10. Parameters for the model were taken from Table 5. The mechanical frequency was set to be 1845 rpm under load. This places the system near the operating point discussed in section 3.3.

## 5.1 Open-Loop Control

The open-loop control method was the first system simulated. The Simulink block diagram of the system is shown in Figure 11. For the given reference signal, (30) yields $u_c$ = -51.15, $u_s$ = 50.36. The results of the simulation are shown in Figure 12.

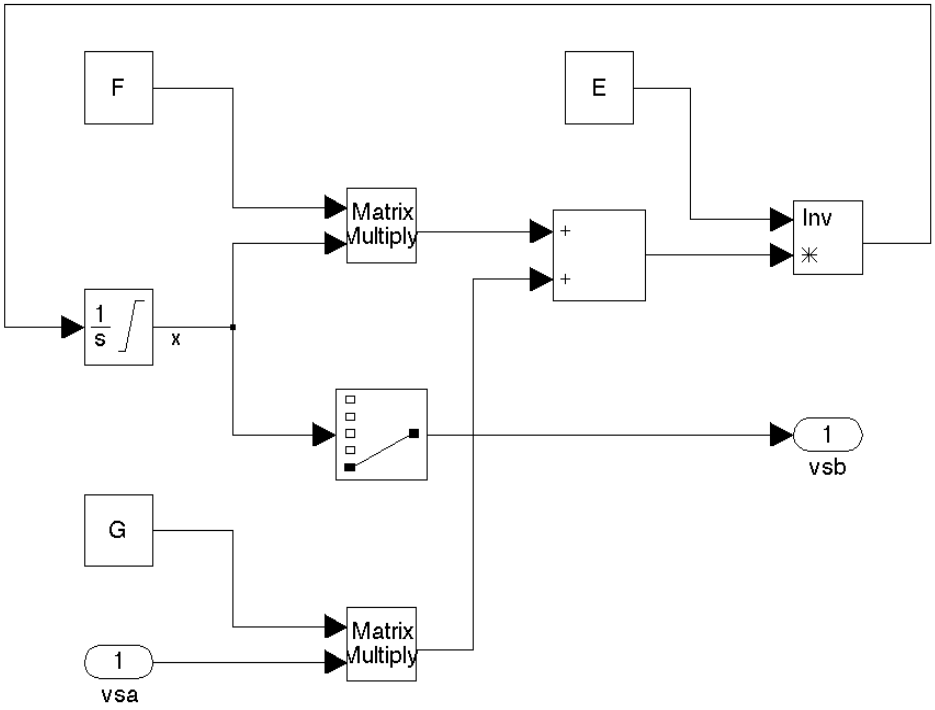


Figure 10: Simulink model of the induction generator

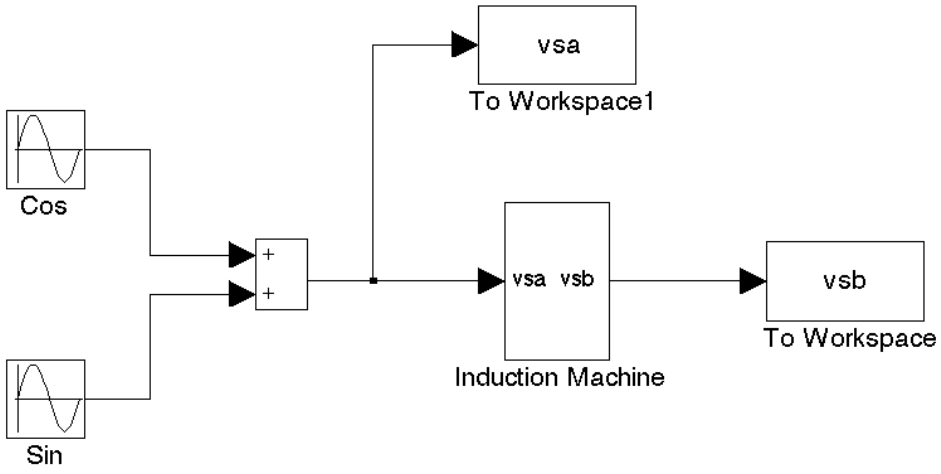


Figure 11: Block diagram of the open-loop control algorithm

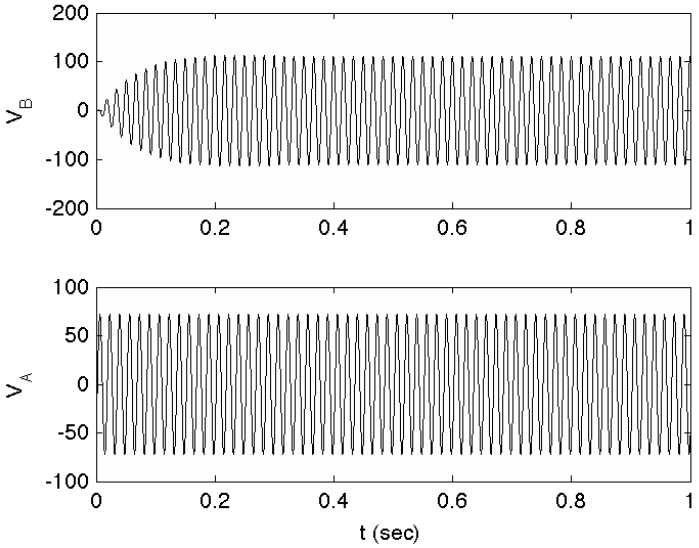


Figure 12: Simulation results of the open-loop algorithm

The simulation produces 110 V across the generating winding as expected. The rise time of the system is approximately 0.1 seconds. The predicted gain of the system can be calculated by measuring the amplitudes of the steady-state voltages.

$$G_{SS}=\frac{\left(V_B\right)}{\left(V_A\right)}=\frac{110}{74.3}=1.48 \tag{55}$$

## 5.2 Adaptive Algorithm for Known Plant

The second algorithm simulated was the adaptive algorithm for known plant introduced in 4.2. The Simulink block diagram of the system is shown in Figure 13. The results of the simulation are shown in Figure 14. The system settles to 110 V as expected. The system is only slightly slower than the open-loop method. It also exhibits more overshoot than the open-loop method. The overshoot can be eliminated by reducing the gain, but this increases the rise time of the system.

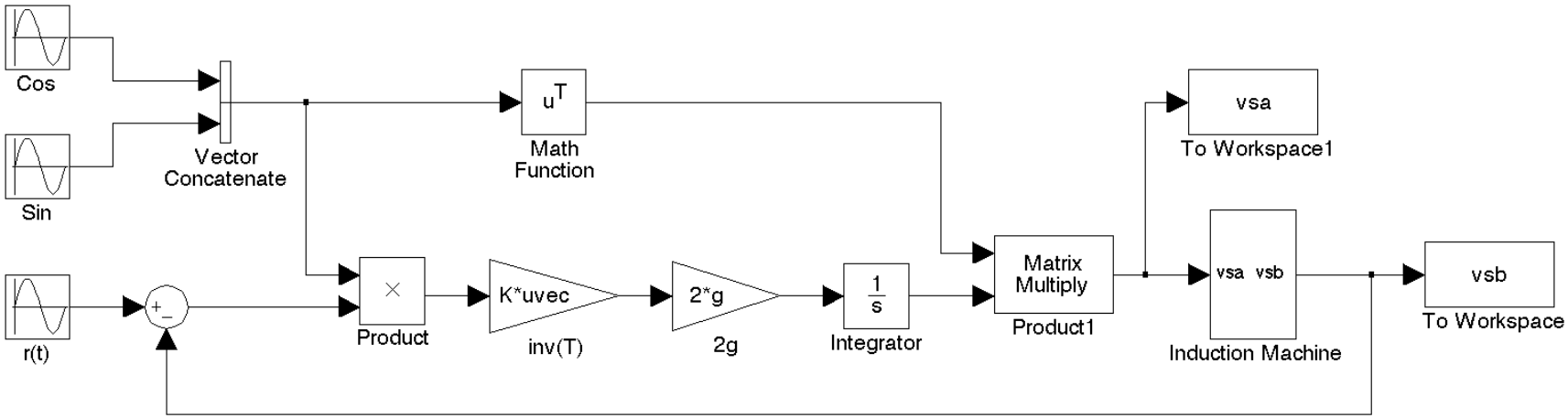


Figure 13: Block diagram of the adaptive algorithm for known plant

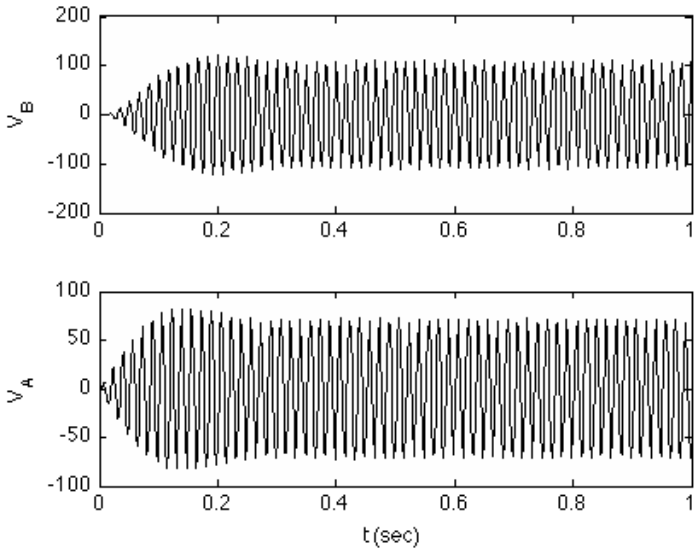


Figure 14: Simulation results of the adaptive method for known plant

## 5.3 Adaptive Algorithm with Plant Adaptation

Next, the algorithm for unknown plant was simulated. This system consists of three subsystems: the induction machine, the error estimator (46) and a gradient descent algorithm (48). A block diagram of the system is shown in Figure 15. The adaptation gain was set to $g = 0.00005$. The results are shown in Figure 16.

Since the plant parameters are initialized exactly, this algorithm converges extremely rapidly. The response will be much slower in practice.

## 5.4 PI Control

Finally, the PI control method discussed in 4.4 was implemented in Simulink. The feedback gains were set to $K_P = 0.5$ and $K_I = 8.5$. The averaging gain was set to $g = 150$. This

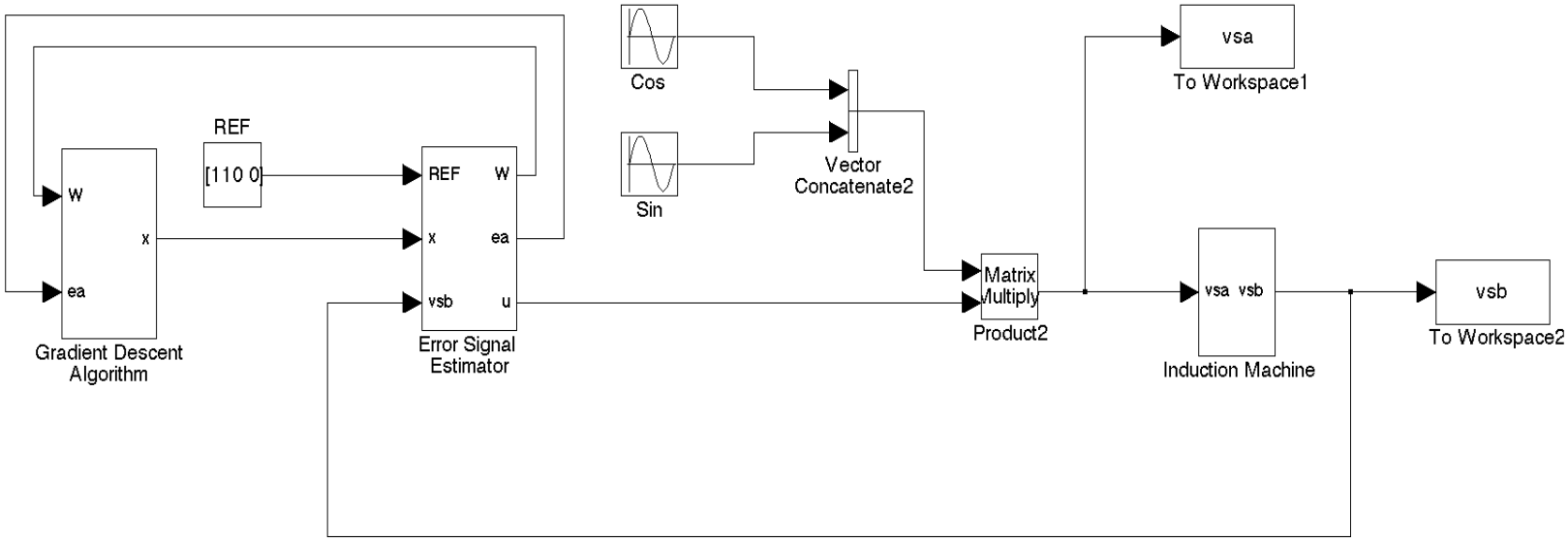


Figure 15: Block diagram of the adaptive algorithm with plant adaptation

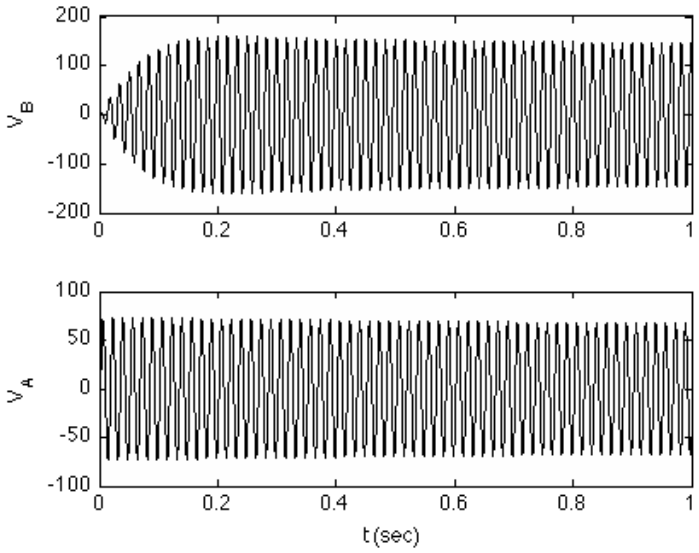


Figure 16: Simulation results of the adaptive method for unknown plant

gain was made much larger than the feedback gains in order to ensure that the dynamics of the averaging filter did not interfere significantly with overall system performance. A block diagram of the system is shown in Figure 17. The results of the simulation are shown in Figure 18. The PI controller responds much more rapidly than the other algorithms - even though the adaptive controllers have exact knowledge of plant parameters.

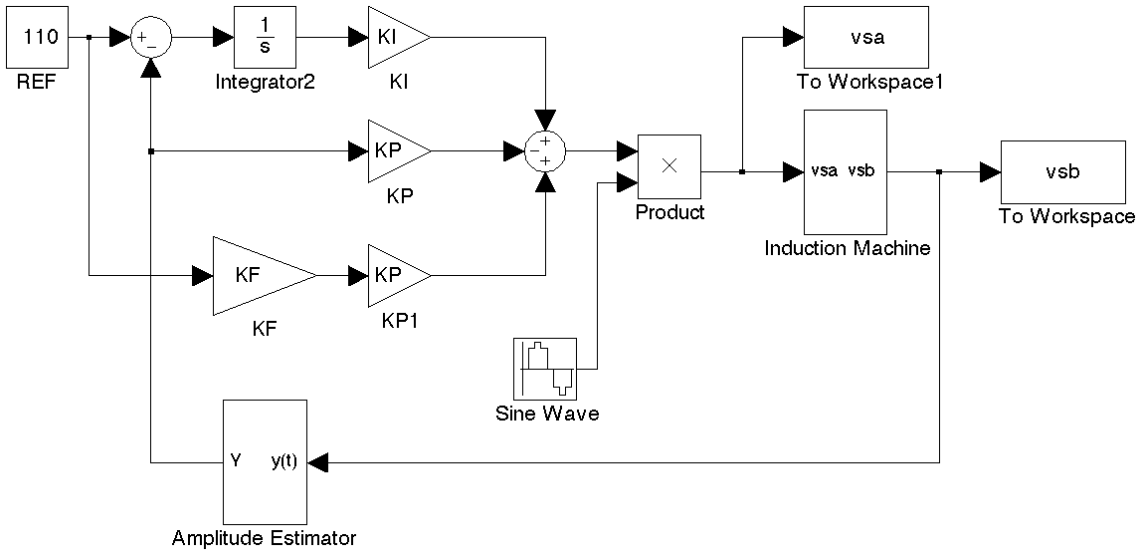


Figure 17: Block diagram of the PI control method

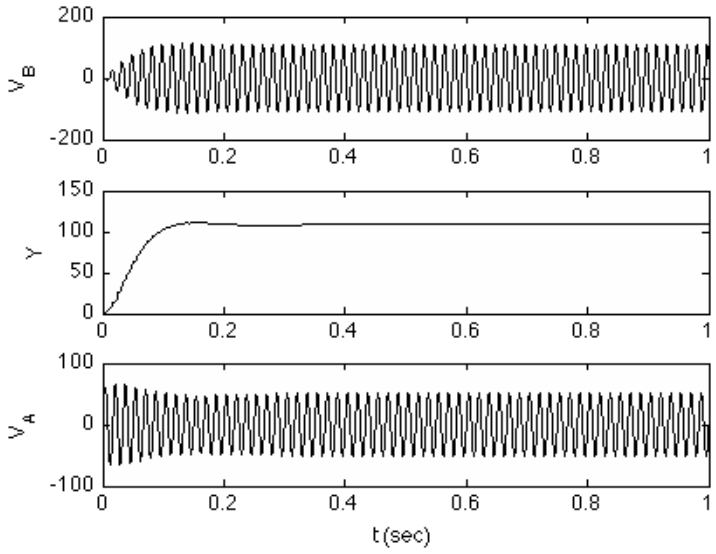


Figure 18: Simulation results of the PI controller

# CHAPTER 6

# EXPERIMENTAL RESULTS

## 6.1 Experimental Setup

An experimental testbed was built in order to test the control methods described in Chapter 4. The testbed consisted of a prime mover connected to a generator via a spider coupling. Both machines were manufactured by the Worldwide Electric Corporation. The prime mover had the nameplate data shown in Table 7. The three-phase voltage required by the prime mover was provided by a GE 300 Mini adjustable frequency drive. The 300 Mini is a V/f drive and therefore the speed of the motor is poorly regulated under varying torque. Figure 19 shows the speed response due to a 110 $V_{pk}$ step in the generated voltage. The measurements were obtained using a Compact Instruments laser tachometer. The data were filtered using a six-pole Butterworth low-pass filter with a 40 Hz cutoff. The filter does not introduce any significant dynamic response. The wringing of the motor drive is evident in many of the experimental responses. This behavior can be eliminated by initializing the speed of the motor nearer its steady-state value. This would mean operating the system farther from the operating point chosen in Chapter 3.

TABLE 7. NAMEPLATE DATA OF PRIME MOVER

| Power | Speed | Phases | Hz | Voltage |
|---|---|---|---|---|
| 1/2 HP | 3450 RPM | 3 | 60 Hz | 208-230/460 V |

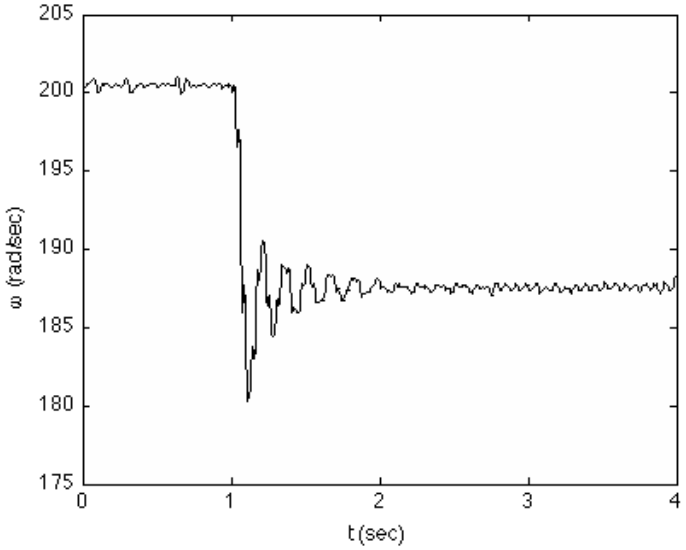


Figure 19: Response of the motor drive system to a step change in torque

The generator under test had the nameplate data shown in Table 8. The start capacitor of the generator was removed in order to provide access to the auxiliary phase of the machine. Both of the machines were fastened to a heavy metal plate for stability. The setup is shown in Figure 20.

The excitation signal was generated using an onboard digital-to-analog converter of a dSPACE DS1104 controller board. This signal was passed to a power amplifier. The generated voltage was measured using the analog-to-digital converter on the DS1104.

In order to compare with the simulations presented in Chapter 5, the speed of the prime mover was set near 1845 rpm under load. This was difficult in practice due to the nature of the drive. As before, the reference was set to $r_c = 110$, $r_s = 0$.

TABLE 8. NAMEPLATE DATA OF GENERATOR UNDER TEST

| Power | Speed | Phases | Hz | Voltage |
|---|---|---|---|---|
| 1/3 HP | 1725 | 1 | 60 | 115/230 V |

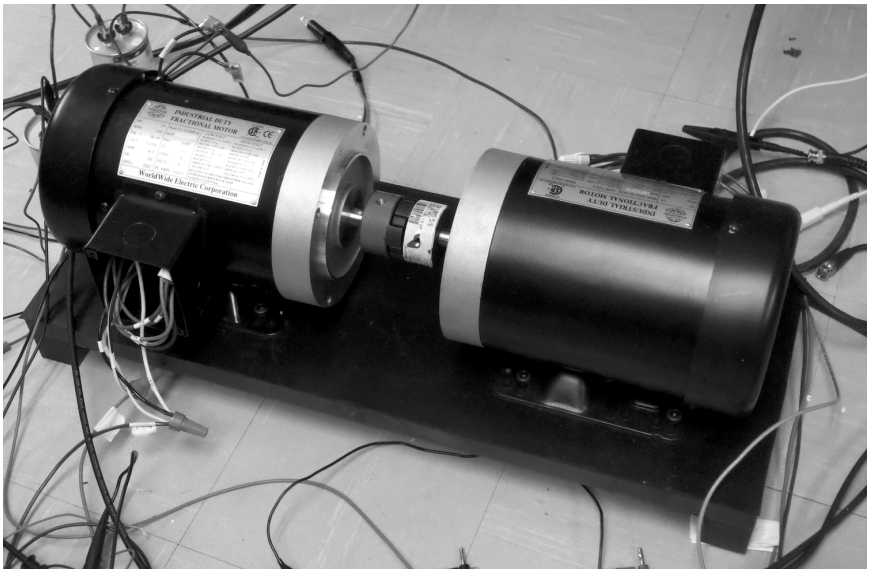


Figure 20: Experimental setup

## 6.2 Open-Loop Control

The open-loop control method was the first implemented. The results of the experiment are shown in Figure 21. An estimate of the amplitude of the generated voltage, *Y*, is included in the plot. The estimate is calculated using (52) and (53), but is not used in the control law. The steady-state gain of the system can be calculated as before

$$G_{SS}=\frac{\left(V_B\right)}{\left(V_A\right)}=\frac{110}{83.9}=1.31 \tag{56}$$

This is approximately 11 percent less than the theoretical value. Note that the model predicts overdamped behavior when the system exhibits slightly underdamped responses. This behavior is due to oscillations in the speed of the generator-motor system.

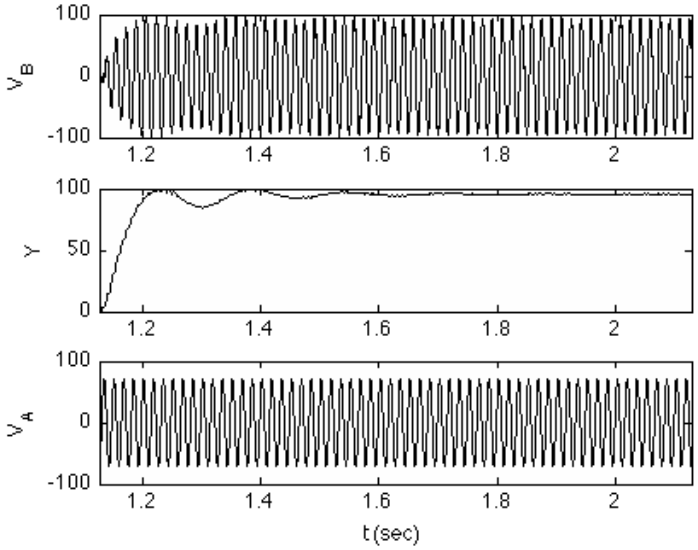


Figure 21: Response of the open-loop control algorithm

## 6.3 Adaptive Algorithm for Known Plant

Next, the adaptive method for known plant was implemented in C and loaded on to the dSPACE system. The adaptation gain was set to $g = 3$. The results are shown in Figure 22. The experiment was repeated at a slower speed to obtain the response shown in Figure 23. Larger gains improve the transient response of the generator, but introduce steady-state oscillations to the output.

It is also informative to examine the response of the algorithm to variations in the plant parameters. The speed of the generator, $\omega$, is the only parameter that can vary significantly during normal operating conditions. The generator was started and allowed to reach steady state at a speed of 1800 rpm. The mechanical frequency was increased to 2160 rpm and the system was allowed to return to steady state. The resulting transients are shown in Figure 24. The maximum voltage deviation is five percent.

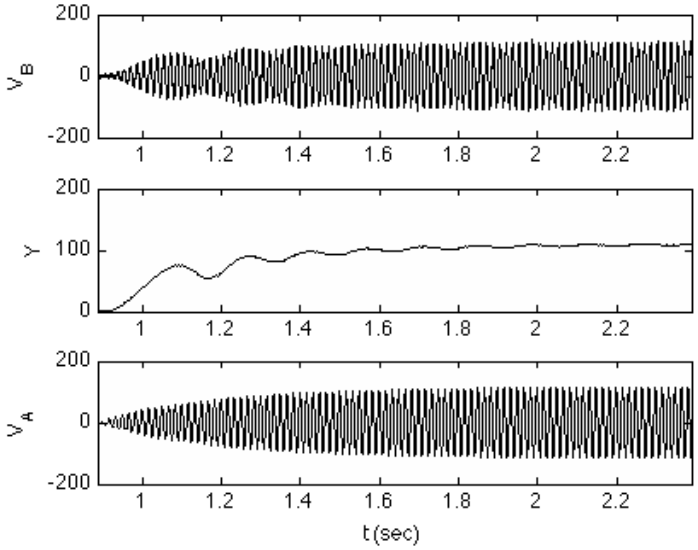


Figure 22: Response of the adaptive algorithm for known plant

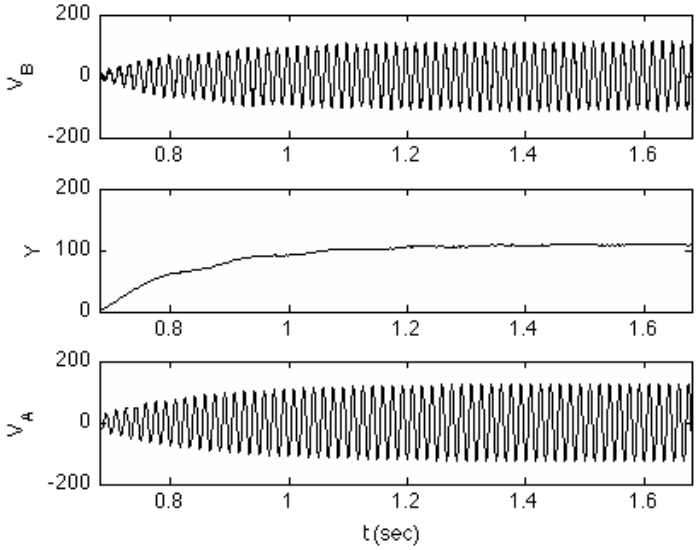


Figure 23: Response of the adaptive algorithm for known plant at slower speed

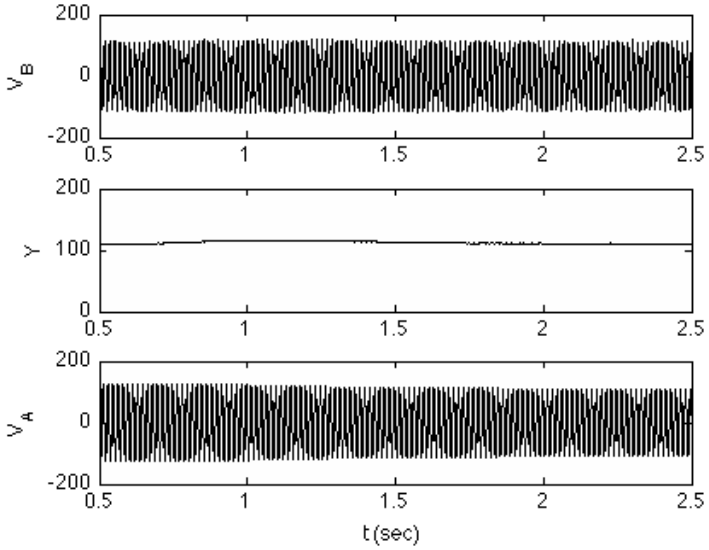


Figure 24: Response of the adaptive algorithm for known plant for a step change in speed at $t = 0.65$ sec.

## 6.4 Adaptive Algorithm with Plant Adaptation

The third experiment implemented on the system was the adaptive algorithm for an unknown plant. The adaptation gain was set to $g = 0.0001$. The initial values of the parameters $x_1$ and $x_2$ were estimated using the real and imaginary parts of the transmittance. The response of the controller to a step reference is shown in Figure 25. The peak overshoot of the controller is approximately 148 V. This is a significant overshoot and could damage connected loads. The adaptive action of this method is apparent in Figure 26. The controller's estimate of the system transfer function converges to $x_1 = -0.54$, $x_2 = -0.77$. A larger adaptive gain causes these estimates to converge quicker, but introduces more overshoot to the system.

The experiments were repeated at a slower speed to reduce drive dynamics. The step response of the controller is shown in Figure 27. The overshoot is reduced to approximately five percent. Once again, the controller's response to a step change in plant parameters was tested by increasing the speed of the generator from 30 Hz to 36 Hz. The results are shown in Figure 28.

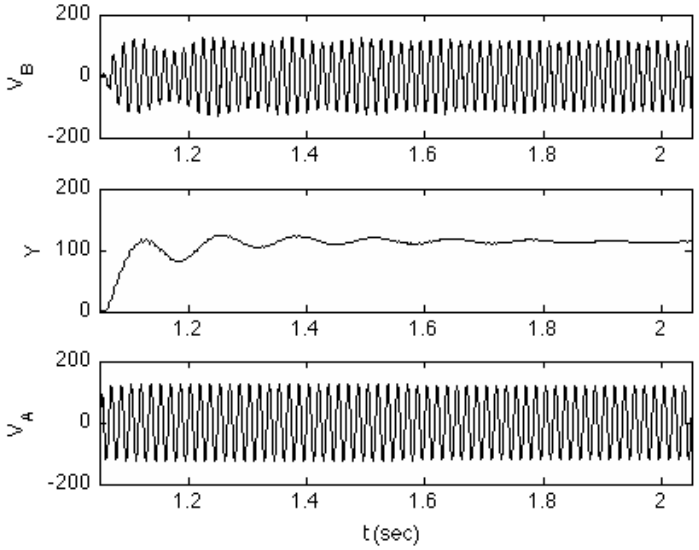


Figure 25: Results of the adaptive algorithm for unknown plant

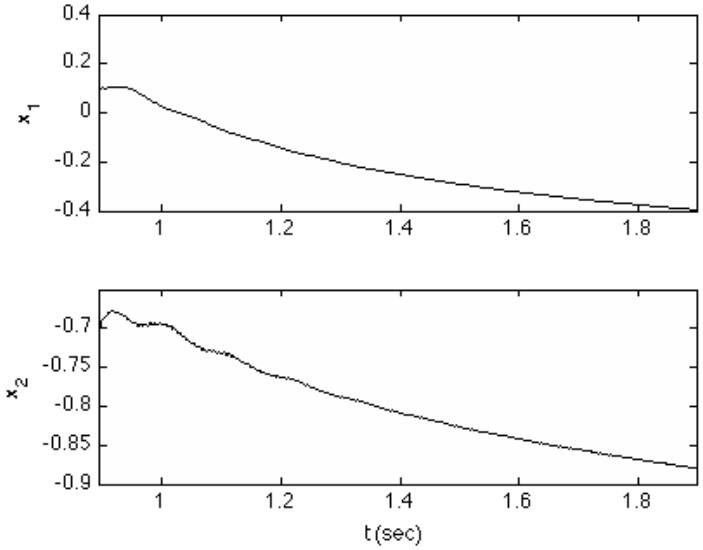


Figure 26: Plant estimates of the adaptive controller for unknown plant

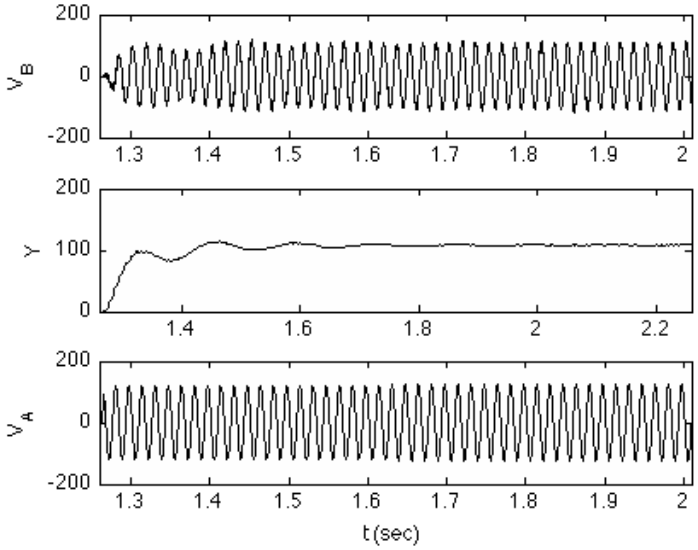


Figure 27: Response of the adaptive algorithm for unknown plant at slower speed

## 6.5 PI Control

The PI control method discussed in section 4.4 was implemented in a similar fashion. The gain used in the amplitude estimator was chosen to be $g = 150$. The selected feedback gains were $k_P = 0.5$ and $k_I = 6.5$. The results of the experiment are shown in Figure 29. Larger values of $g$ increase the response time and decrease the maximum overshoot. However, if $g$ is too large it causes steady-state oscillations in the output voltage. Once again, the experiment was repeated at a slower speed. The results of the slower experiment are shown in Figure 30. The rise time of the response is in good agreement with the simulation presented in Figure 18.

The response of the PI controller to a change in the plant parameters was also investigated. Figure 31 shows the response of the system to a 20 percent increase in speed at $t =$ 1.5 sec. Since the action of the controller is faster than the acceleration of the prime mover, there is no significant change in the generated voltage.

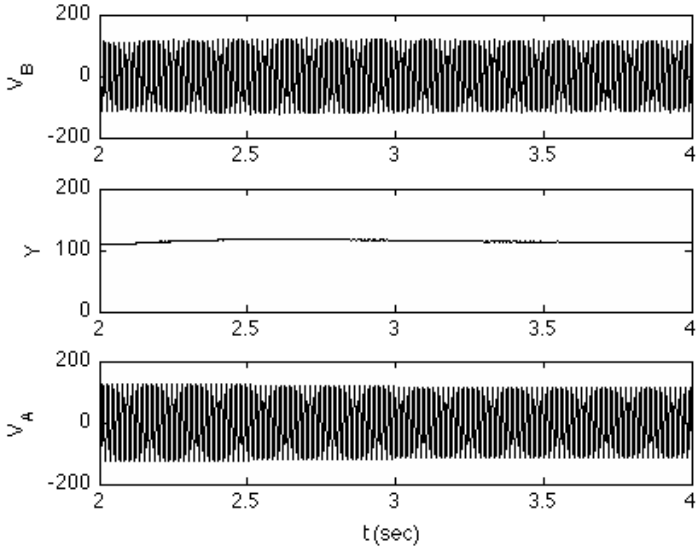


Figure 28: Response of the adaptive algorithm for unknown plant to step change in speed

A final experiment was performed to examine the behavior of the generator under different loading conditions. The 100 Ω load resistor was replaced with a universal motor. The reactive power requirements of the motor are more typical of residential loads. Figure 32 shows the response of the system to a step in voltage. The inductance of the motor coils allows the load to increase gradually, eliminating some of the overshoot. The same gains were used for each of the experiments.

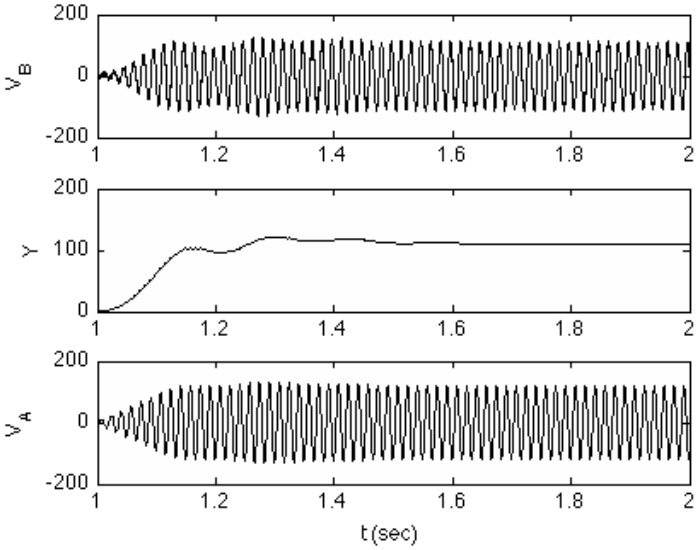


Figure 29: Response of the PI controller

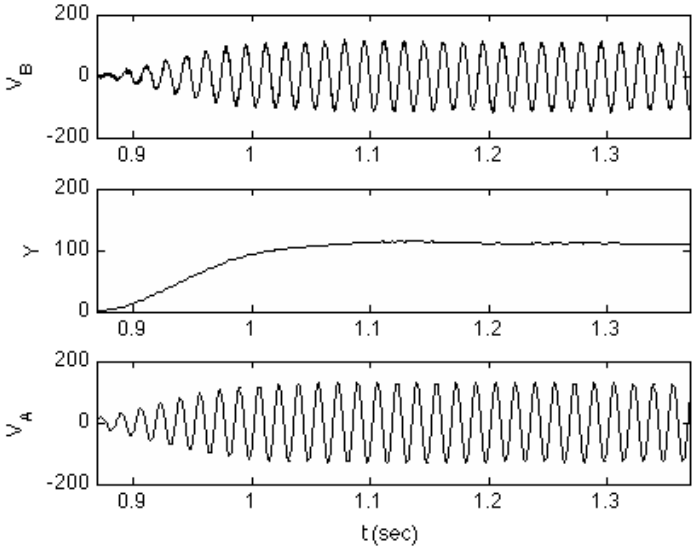


Figure 30: Response of the PI controller at slower speed

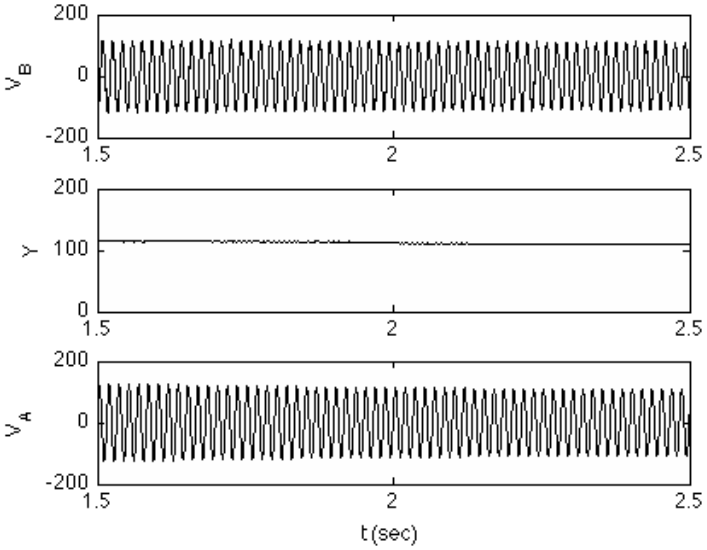


Figure 31: Results of the PI controller to a step change in speed

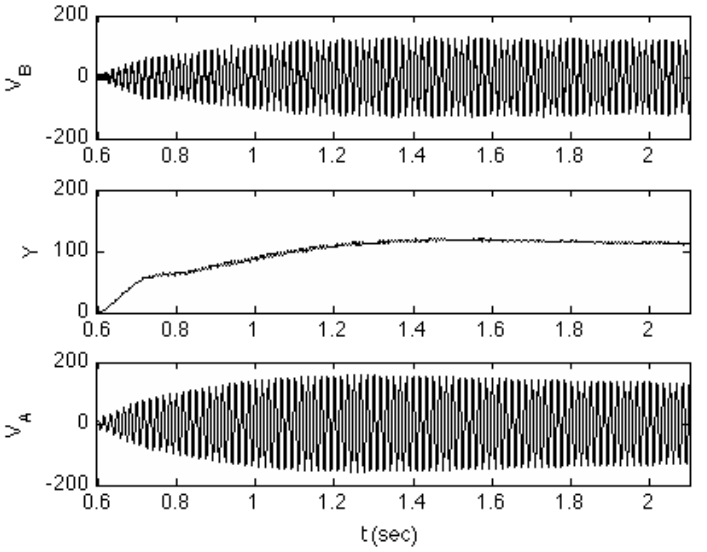


Figure 32: Response of the PI controller with an inductive load

# CHAPTER 7

# CONCLUSIONS

This thesis examined the problem of producing a controlled voltage from a single-phase induction machine. A state-space model of a SPIM was presented. The parameters of a symmetric induction machine were obtained by fitting data to this model. These estimates were in good agreement with measurements taken using standard tests. The method was used to identify the parameters of each phase of an asymmetric induction machine.

In order to predict power generation, the state-space model was expanded to include an RC load connected across the main phase. The identified parameters were used to estimate the operating region. It was concluded that power can be produced in a limited region above the synchronous speed of the motor. Power is produced by both phases of the machine in most of the operating region. The point $P_A = 0$ was chosen as the operating point in order to eliminate costly power electronics.

Finally, four control methods were investigated. The three closed-loop algorithms were able to reliably track a reference voltage. Furthermore, each control algorithm was robust to a 20 percent increase in speed. In practice, the adaptive algorithm for unknown plant was faster than the adaptive algorithm for known plant. Variations in the speed of the system caused dangerous transients when the adaptive algorithm for known plant was used. In both cases, the adaptation gain can be increased to speed up the response, but this comes at the cost of greater transients on the line. In situations where phase is not a consideration, the PI control method is preferable. It responds faster than either adaptive method.

Further research could focus on methods to improve the transient response of the

generator. This could be done by incorporating some form of closed-loop speed control, allowing the system to remain near its optimal operating speed. Alternately, the system could employ closed-loop current control. This would allow the current to be gradually increased, improving the transient performance of the drive.

# REFERENCES


[1] D. W. Novotny, D. J. Gritter, & G. H. Studman, "Self-Excitation in Inverter Driven Induction Machines," *IEEE Trans. on Power Apparatus and Systems*, vol. 96, no. 4, 1977, pp. 1117–1125.

[2] S.S. Murthy, "A Novel Self-Excited Self-Regulating Single-Phase Induction Generator, Part I and II," *IEEE Trans. on Energy Conversion*, vol. 8, no. 3, September 1993, pp. 378-388.

[3] O. Ojo, "The Transient and Qualitative Performance of a Self-Excited, Single-Phase Induction Generator," *IEEE Trans. on Energy Conversion*, vol. 110, no. 3, September 1995, pp. 493-501.

[4] O. Ojo & B. Gonoh, "A Controlled Stand-Alone Single-Phase Induction Generator," *Power Electronics, Drives and Energy Systems for Industrial Growth*, vol. 2, no. 8, January 1996, pp. 694-699.

[5] O. Ojo, "Performance of Self-Excited Single-Phase Induction Generators with Shunt, Short-Shunt and Long-Shunt Excitation Connections," *IEEE Trans on Energy Conversion*, vol. 11, no. 3, September 1996, pp. 477-482.

[6] O. Ojo, O. Omozusi, & A. A. Jimoh, "Performance of an Autonomous Single-Phase Induction Generator with a Bidirectional PWM Inverter-Battery System in the Auxiliary Winding," *IEEE International Symposium on Industrial Electronics*, vol 1, no. 7, July 1998, pp 306-311.

[7] O. Ojo, O. Omozusi, A. Ginart, & B. Gonoh, "The Operation of a Stand-Alone Single-Phase Induction Generator using a Single-Phase, Pulse-Width Modulated Inverter with a Battery Supply," *IEEE Trans. on Energy Conservation*, vol. 14, no. 3, September 1999, pp. 526-531.

[8] O. Ojo, "The Operation of an Inverter-Assisted Single-Phase Induction Generator," *IEEE Trans. on Industrial Electronics*, vol. 47, no. 3, June 2000, pp 632-640.

[9] O. Ojo, O. Omozusi, M. Omoigui, & A. A. Jimoh, "Parameter Estimation of Single-Phase Induction Machines," *Conference Record of the 2001 IEEE Industry Applications Conference*, 2001, pp. 2280–2287.

[10] C. van der Merwe & F. S. van der Merwe, "A Study of Methods to Measure the Parameters of Single-phase Induction Motors," *IEEE Trans. on Energy Conversion*, vol. 10, no. 2, 1995, pp. 248–253.

[11] F. Suhr, "Towards an Accurate Evaluation of Single-phase Induction Motor Constants," *Trans. AIEE Part 3, Power Apparatus and Systems*, vol. 71, 1952, pp. 221–227.

[12] A. Gastli, "Identification of Induction Motor Equivalent Circuit Parameters Using the Single-Phase Test," *IEEE Trans. on Energy Conversion*, vol. 14, no. 1, 1999, pp. 51– 56.

[13] W. Chen, D. Xu, G. Wang, Y. Yu, & C. C. Chan, "Parameters Estimation of Induction Motor at Standstill Concerning the Nonlinearity of the System," *Vehicle Power and Propulsion*

*Conference*, 2009, pp. 1407– 1411.

[14] R. P. Vieira, R. Z. Azzolin, & H. A. Gründling, "Parameter Identification of a Single-Phase Induction Motor Using RLS Algorithm," *Power Electronics Conference*, 2009, pp. 517–523.

[15] V. Hrabovcova, L. Kalamenm P. Sekerak, & P. Rafajdus, "Determination of Single Phase Induction Motor Parameters," *Proc. of the 20th International Symposium on Power Electronics, Electrical Drives, Automation and Motion*, 2010.

[16] B. Wu & M. Bodson, "Multi-Channel Active Noise Control for Periodic Sources – Indirect Approach," *Automatica*, vol. 40, no. 2, 2004, pp. 203-212.

[17] S. Pigg & M. Bodson, "Adaptive Rejection of Sinusoidal Disturbances of Known Frequency Acting on Unknown Systems," *Proc. of the American Control Conference*, 2006, 4777 – 4781.